Nanopatterned Textile-Based Wearable Triboelectric Nanogenerator

Wanchul Seung,[†] Manoj Kumar Gupta,[†] Keun Young Lee,[†] Kyung-Sik Shin,[†] Ju-Hyuck Lee,[‡] Tae Yun Kim,[‡] Sanghyun Kim,[†] Jianjian Lin,[§] Jung Ho Kim,[§] and Sang-Woo Kim*[,†,‡]

[†]School of Advanced Materials Science and Engineering and [‡]SKKU Advanced Institute of Nanotechnology (SAINT), Center for Human Interface Nanotechnology (HINT), Sungkyunkwan University, Suwon 440-746, Republic of Korea and [§]Institute for Superconducting and Electronic Materials (ISEM), Australian Institute for Innovative Materials (AIIM), University of Wollongong, North Wollongong, NSW 2500, Australia

ABSTRACT Here we report a fully flexible, foldable nanopatterned wearable triboelectric nanogenerator (WTNG) with high power-generating performance and mechanical robustness. Both a silver (Ag)-coated textile and polydimethylsiloxane (PDMS) nanopatterns based on ZnO nanorod arrays on a Ag-coated textile template were used as active triboelectric materials. A high output voltage and current of about 120 V and 65 μA, respectively, were observed from a nanopatterned PDMS-based WTNG, while an output voltage and current of 30 V and 20 μA were obtained by the non-nanopatterned flat PDMS-based WTNG under the same compressive force of 10 kgf. Furthermore, very high voltage and current outputs with an average value of 170 V and 120 μA, respectively, were obtained from a four-layer-stacked WTNG under the same compressive force. Notably it was found there are no significant differences in the output voltages measured from the multilayer-stacked WTNG over 12 000 cycles, confirming the excellent mechanical durability of WTNGs. Finally, we successfully demonstrated the self-powered operation of light-emitting diodes, a liquid crystal display, and a keyless vehicle entry system only with the output power of our WTNG without any help of external power sources.

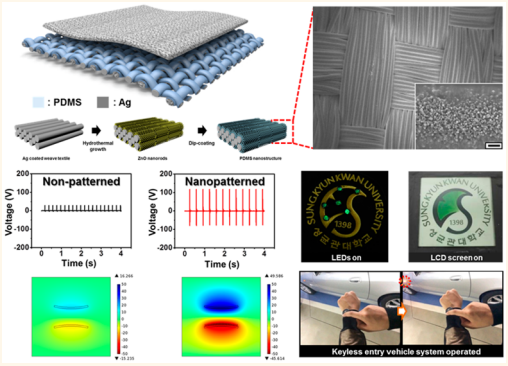

KEYWORDS: nanopattern · triboelectricity · nanogenerator · self-powering · wearable electronics

Textile-based devices have gained tremendous attention due to their excellent flexibility, high sustainability, light weight, comfort, and wide-ranging applications such as wearable electronic devices, robotic sensory skins, and biomedical devices.[1−4] In particular, wearable electronic devices are different from existing mobile gadgets, including smartphones and tablets, which look and feel similar to one another, indicating that the devices not only have to be functional but have to be well designed as well. Further, to reduce the size and weight of a wearable device, it is inevitable that a novel wearable energy source with high flexibility, high mechanical robustness, light weight, and large power output has to be integrated with the textile platform. The wearable devices require their own power sources. In most cases, the power source is a conventional electrochemical battery. However, even if the battery has a huge capacitance, it has a limited lifetime. Furthermore, flexible and stretchable batteries to be integrated with the textile suffer from very low mechanical durability and very short battery lifetimes. In these regards, nanogenerators (NGs) have been regarded as an important new type of energy-harvesting technology that converts mechanical energy into electrical energy and have attracted great attention for realizing self-powered wearable electronics.[5−12]

Recently, new types of simple, reliable, and cost-effective triboelectric NGs (TNGs) have been successfully developed and used to harvest mechanical energy.[13−32] In principle, surface charge is transferred when two materials with different triboelectric polarities are contacted/rubbed together; when they separate, a dipole moment is developed, which drives electrons through external loads on the basis of both triboelectric and electrostatic effects. The output power of TNGs has been successfully used for self-powering various kinds of sensors and mobile electronics with low power consumption.[14,33−35] The surfaces

* Address correspondence to kimsw1@skku.edu.

Received for review December 18, 2014 and accepted February 10, 2015.

Published online February 11, 2015
10.1021/nn507221f

of triboelectric materials are often modified to enhance the friction and surface area. Although various types of nanostructures such as nanoparticles, nanorods, and nanowires are decorated into TNGs to increase the contact area between two friction surfaces for obtaining large power generation from the TNGs, the TNGs with nanostructured surfaces are fabricated on a plastic platform rather than a textile one for wearable electronics.[13,14,36] Hence, a low-cost but simple approach for nanopatterning on triboelectric-active materials with a textile platform is crucial to realize the full potential of TNGs.

Commercially available metal-coated textile materials have emerged as promising substrates for a wide range of wearable electronic device applications due to their excellent mechanical strength, light weight, flexibility, foldability, stretchability, good machinability, and low cost. For highly efficient WTNGs, triboelectric nanopatterns with large surface area on textiles are greatly desirable. However, to the best of our knowledge, there has been no report on nanopatterned textile-based wearable TNGs (WTNGs) with very high mechanical robustness by bottom-up nanostructuring due to very weak adhesion between the textile and nanostructure, causing mechanical durability issues. Therefore, it remains a sizable challenge to nanostructure a metal-coated textile that is both chemically and physically damage-free.

Herein we demonstrate a new type of fully flexible, foldable nanopatterned WTNG with high power-generating performance and mechanical robustness for the first time. Both a silver (Ag)-coated textile and polydimethylsiloxane (PDMS) nanopatterns based on ZnO nanorod (NRs) arrays on a Ag-coated textile template were used as active triboelectric materials. Nanopatterning was achieved by coating PDMS directly over vertical ZnO NRs grown on the Ag-coated textile substrate. A high output voltage and output current of about 120 V and 65 μA, respectively, were observed from a nanopatterned PDMS-based WTNG, while an output voltage and output current of 30 V and 20 μA were obtained by the non-nanopatterned flat PDMS-based WTNG under the same mechanical compressive force. Furthermore, it was found that the electric power output can be effectively increased by the multilayered vertical staking of the WTNG with ease. Very high voltage and current outputs with an average value of 170 V and 120 μA, respectively, were obtained from the four-layer-stacked WTNG. The output power was maximized at around 1.1 mW at an external resistance of about 1 MΩ. Notably, it was found that there are no significant differences in the output voltages measured from the multilayer-stacked WTNG over 12 000 cycles, confirming the excellent mechanical durability of WTNGs. Finally, we successfully demonstrated the self-powered operation of light-emitting diodes (LEDs), a liquid crystal display (LCD), and a keyless vehicle entry system only with the output power of our WTNG without any help from external power sources.

RESULTS AND DISCUSSION

Schematic images in Figure 1a and b present the fabrication process of the fully flexible and foldable WTNG. ZnO NR array-templated PDMS nanopatterns acting as a triboelectric active layer at the bottom side were synthesized on a Ag-coated textile substrate using a hydrothermal growth method of ZnO and a dip-coating process of a PDMS solution. The top Ag-coated textile was utilized as a flexible and foldable substrate as well as a triboelectric-active material. No additional spacer was used between the textile and the nanopatterned PDMS. Nanopatterning promotes the triboelectrification effect by increasing the effective contact area and friction during contact and separation of the textile and PDMS.

Figure 1c is a field-emission scanning electron microscopy (FE-SEM) image of the nanopatterned PDMS on the plain weave textile coated with Ag. The FE-SEM analysis of the PDMS-coated ZnO NR sample was carried out to investigate the fine features within the structure, as shown in the inset of Figure 1c. It is clearly shown in the FE-SEM image that the PDMS nanopatterns were successfully fabricated on the textile substrate with the help of the ZnO NR template. FE-SEM images of the Ag-coated knitted woven textile top electrode are shown in Figure S1. The FE-SEM images in Figure S2 reveal uniformly well-aligned ZnO NRs on the textile substrate. The average diameter and length of the ZnO NRs were 100 nm and 1 μm, respectively. A photographic image (Figure 1d) shows the high flexibility and foldability of the WTNG with the nanopatterned PDMS on the Ag-coated textile substrate.

In order to compare the electric power output performance, we also fabricated a WTNG without the nanopatterned PDMS film, *i.e.*, a flat PDMS and a top Ag-coated textile electrode as the opposite triboelectric material. The output voltage and current generated from both the WTNGs were measured by applying compressive force (10 kgf) perpendicular to the WTNGs using a mechanical force stimulator. An output voltage of approximately 30 V was observed with an output current of 20 μA from the flat PDMS-based WTNG (Figure 2a and b), while the nanopatterned WTNG produced a very high output voltage and current, with average values of 120 V and 65 μA, respectively, under the same compressive force of 10 kgf (Figure 2c and d). The large enhancement in the output voltage and current is attributed to the increase in friction achieved *via* the nanopatterned PDMS structure.

Polarity-switching tests were also carried out to confirm that the output electric signals originated from the WTNG rather than the measurement system (see Supporting Information, Figure S3). An opposite

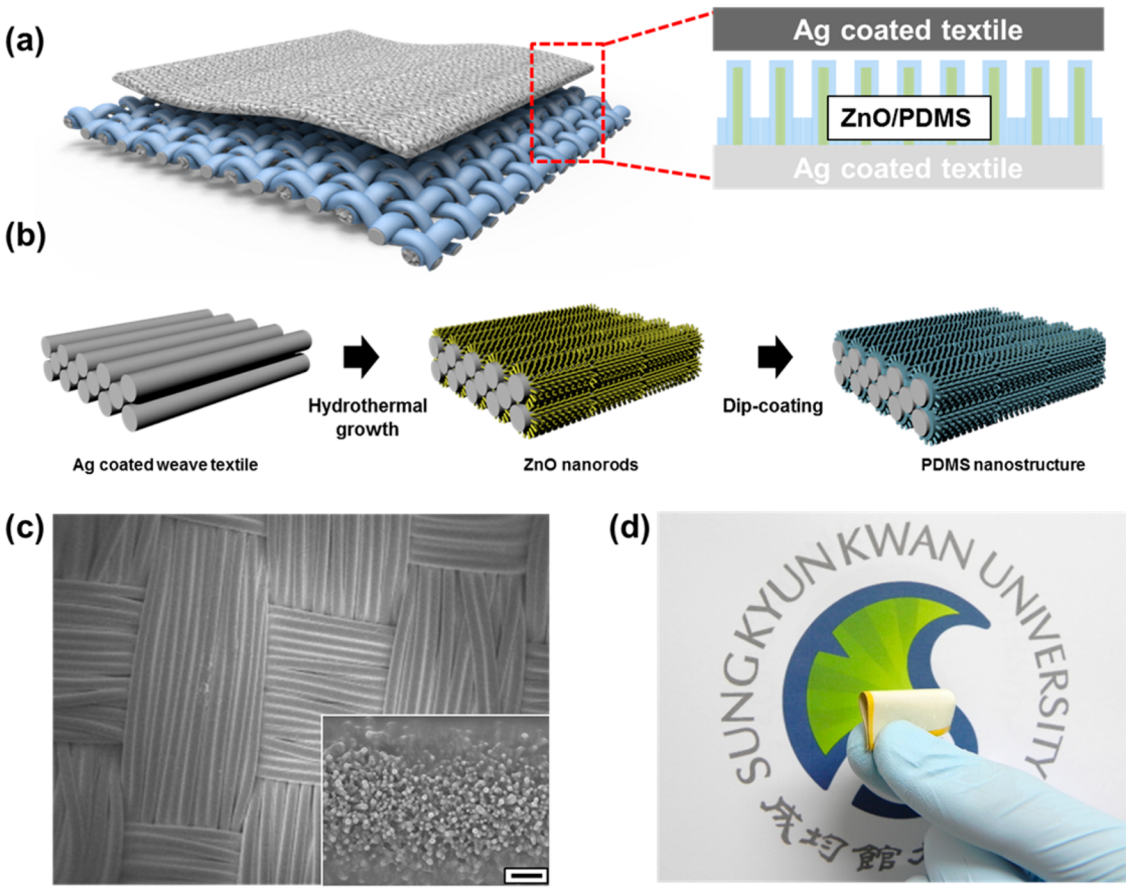

Figure 1. (a) Schematic illustration of the WTNG. (b) Fabrication process of the nanopatterned PDMS structure. (c) FE-SEM images of the bottom textile with nanopatterned PDMS. Inset is a high-resolution image clearly showing the ZnO NR-templated PDMS nanopatterns. (d) Photographic image of the flexible, foldable WTNG.

output signal is observed when the WTNG is connected in reverse connection. The observed large electric power output is several times higher than the output power of other textile-based NGs.[37−42] It should be noted that the output power obtained from the nanopatterned PDMS-based WTNG is sufficient to power small-scale electronic devices with low power consumption. In addition, the COMSOL package was used to investigate the triboelectric charge distribution in the flat and nanopatterned WTNGs under the same compressive force. It was found that the triboelectric-induced charge potential is dramatically increased by nanopatterning, as shown in Figure 2e and f. The potential distribution in the flat and nanopatterned WTNGs reveals good agreement between the results obtained from experiments and simulations.

The charge generation mechanism of the WTNG based on the conductive flexible Ag-coated textile and nanopatterned PDMS in the contact−separation due to the cyclic application and release of a load is illustrated in Figure 3. It is well known that a periodic contact and separation between two materials with opposite triboelectric polarities drives electrons back and forth through an external circuit due to the coupling of the triboelectric effect and the electrostatic effect.[13] The charge transfer characteristic between Ag and PDMS strongly depends on their relative positions in the triboelectric series. In the present device configuration, initially the device remained neutral in the absence of any external force (Figure 3a). Further, when a compressive force is applied to the top surface of the device, the Ag-coated textile and the nanopatterned PDMS film are rubbed together. At this time triboelectric charges with opposite signs are generated depending on the position in the triboelectric series. Electrons are injected into the PDMS film from the conductive Ag textile, which results in the Ag-coated textile becoming positively charged and the PDMS becoming negatively charged (Figure 3b).

Once the textile and the nanopatterned PDMS film are separated from each other, the dipole moment becomes stronger. In order to maintain the original state of electrostatic equilibrium, electrons flow from the bottom electrode to the Ag-coated textile electrode; then an electric signal is observed (Figure 3c). The equilibrium stage is shown in Figure 3d, and no electrical signal is observed at this stage. It is worth pointing out that an effective dipole moment can form without any need for an additional spacer between the PDMS and the top textile due to the naturally formed

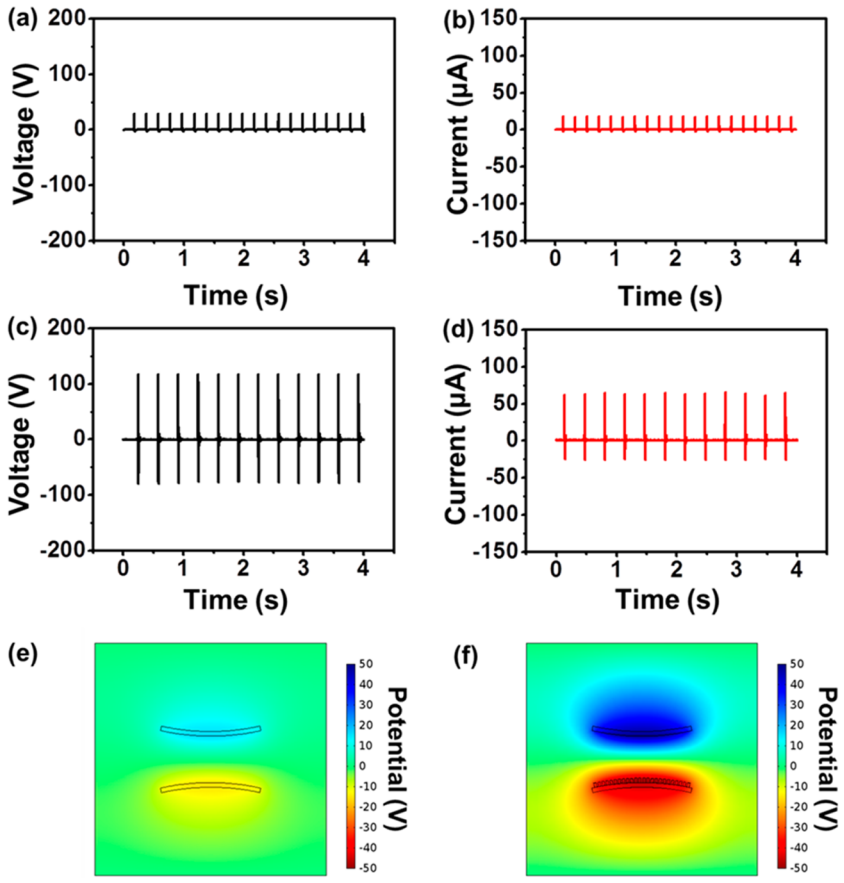

Figure 2. Electrical power output performances of the WTNGs. (a, b) Output voltage and current from the flat PDMS-based WTNG, respectively. (c, d) Output voltage and current from the nanopatterned PDMS-based WTNG, respectively. The potential distributions of (e) the flat PDMS-based WTNG and (f) the nanopatterned PDMS-based WTNG obtained by the COMSOL Multiphysics software.

significant gap that originates from the inherent elasticity of the materials. When the Ag-coated textile and the PDMS surfaces are rubbed together with subsequent application of pressure, the dipole moment is diminished. Thus, the electrons accumulated on the upper side flow back to the bottom electrode side, and an electric signal in the opposite direction is observed (Figure 3e). Therefore, continuous application and release of an external load can generate a complete cycle of alternating current electric signal, as shown in the inset of Figure 3.

To further enhance the total power output, a multilayer-stacked WTNG is demonstrated. In this design, PDMS nanopatterns based on ZnO NRs formed *via* a dip-coating process were synthesized on both sides of the Ag-coated textile substrate. A schematic image of the multilayer-stacked WTNG is displayed in Figure 4a. In order to realize a stacked structure, initially both sides of the nanopatterned PDMS were placed on the top of a single cell of WTNG. The multilayer-stacked structure of WTNG was finally obtained by adding another single cell of WTNG. The double-sided nanopatterned PDMS is sandwiched with two Ag-coated textiles. Thus, the multilayer-stacked WTNG device has four active single WTNG units. To evaluate the power output performance of the multilayer-stacked WTNG, we measured the output voltage and current by applying a pushing force to the top of the WTNG in the vertical direction. The voltage and current output were measured as a function of the number of stacks (Figure 4b). The voltage and current output increased linearly with the number of stacks. Interestingly, very high voltage and current outputs with an average value of 170 V and 120 μA, respectively, were obtained from the four-layer-stacked WTNG under a normal compressive force of 10 kgf. It is clear that the output voltage and current from the multilayer-stacked WTNG were greatly enhanced compared to those of the single-cell WTNG. The higher output performance with the increase in the number of layers is attributed to the parallel connections of WTNGs and the generation of high surface triboelectric charges.

Furthermore, the electric output signals from the stacked WTNG were achieved at different forces ranging from 0.1 to 15 kgf (Figure 4c). It was found that there is steep increase of output voltage as a function of the applied force below 1 kgf (the region indicated as R(i)), and in the range from 1 to 10 kgf, the output voltage and current increase linearly with the applied force, reaching maximum values of about 170 V and

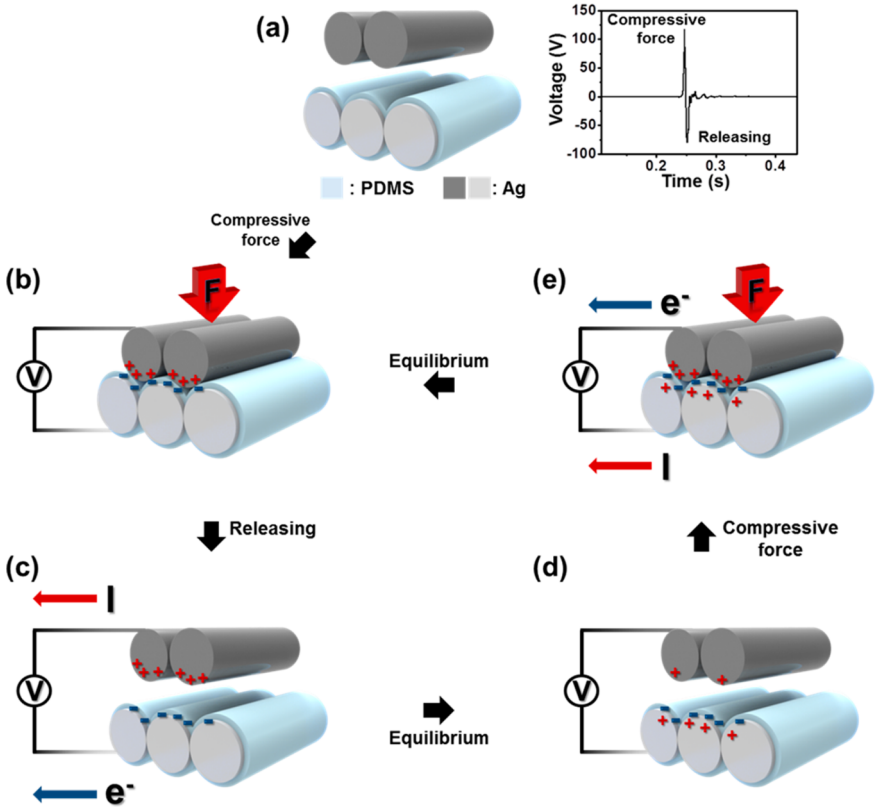

Figure 3. Power generation mechanism of WTNG. (a) The initial state of the device remains neutral in the absence of any external force. (b−e) Schematic illustration showing the suggested working principle of the WTNG with electron and current flow diagrams.

120 μA, respectively (the region indicated as R(ii)). On the other hand, no further significant increase of electric output was observed over the applied force of 10 kgf (the region indicated as R(iii)). A larger applied force leads to the formation of a larger contacting area, indicating the generation of higher density triboelectric charges on the triboelectric active layers of Ag and PDMS.[43] The saturation in electric power output beyond the critical force is due to the limited capability of surface charge generation by triboelectrification. The actual voltage and current output results obtained from the four-layer-stacked WTNG with variation of the applied force are presented in Figure S4. We further explored the output voltages with continuous application of cycled compressive force to the four-layer-stacked WTNG. Notably, there were no significant differences in the output voltages measured from the multilayer-stacked WTNG over 12 000 cycles (Figure 5), confirming the excellent mechanical durability of our WTNG in this work. The strain distributions of ZnO NR arrays and ZnO NR array-templated PDMS nanopatterns on the same Ag-coated textiles were simulated as shown in Figure S5. Strain fields generated by applying a vertical compressive force are mainly localized at both the top and bottom of the ZnO NRs, while they are uniformly distributed over the entire ZnO NRs with the help of a PDMS coating, resulting in the stable power-generating performance of the WTNG with PDMS nanopatterns.

The output voltage and current from the stacked WTNG were systematically measured using different resistors as external loads (Figure 6a). The output current decreases with increasing resistance, while the output voltage follows a reverse trend. The corresponding output power of the stacked WTNG was also plotted as a function of external resistance (Figure 6b). The results show that the output power increases at a low resistance and then decreases at a higher resistance. The output power is maximized at around 1.1 mW at an external resistance of about 1 MΩ. Further, in order to build a complete power package to continuously power small-scale electronic systems by the WTNG, the electric charge output was stored in a capacitor. To demonstrate the charging behavior by the WTNG, two capacitors with values of 3.3 and 10 μF were used for electric energy storage. A rectification circuit was used to convert the alternate current signal into a direct current signal. The charging curves of the capacitors charged by the power generated from the stacked WTNG are shown in Figure 6c. The results confirm that the WTNG takes 20 s to charge the 10 μF capacitor to 2 V and the 3.3 μF capacitor to 7 V under an application of a compressive force normal to the WTNG.

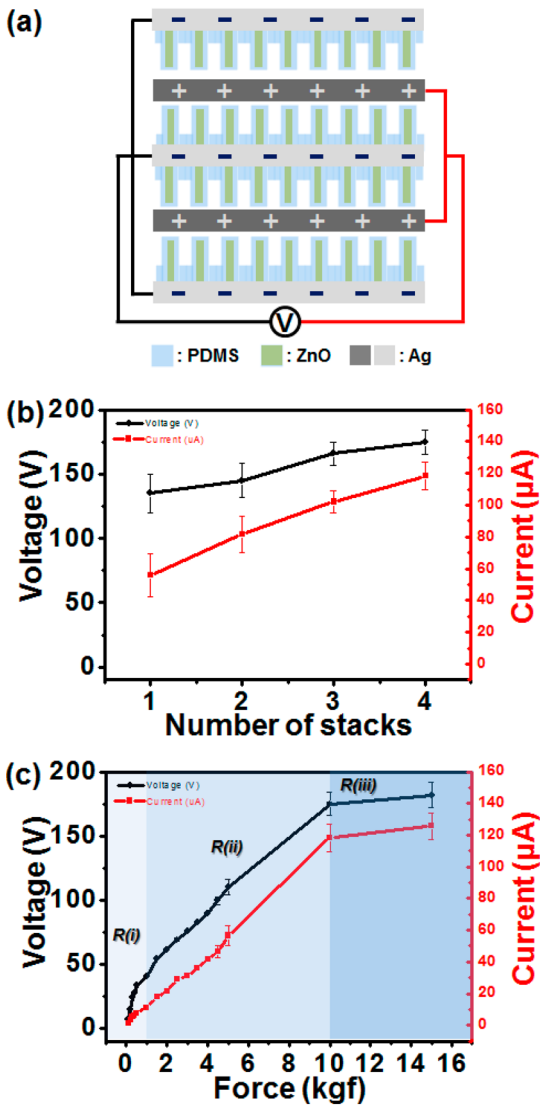

Figure 4. (a) Schematic image of the multilayer-stacked WTNG. (b) Voltage and current outputs measured as a function of the number of stacks by applying a pushing force to the top of the WTNG in the vertical direction. (c) Electric output signals obtained from the stacked WTNG at different forces ranging from 0.1 to 15 kgf.

To demonstrate the application of the WTNG as a power source to drive personal wearable electric devices/systems, we embedded LCD, LEDs, and a remote control (keyless vehicle entry system) in "the self-powered smart suit". We directly powered six LEDs connected in series, an LCD, and a remote control, using the output power of the WTNG. The flexibility of the device enabled a multilayer-stacked WTNG to be affixed to a commercially available jacket as shown in Figure 7. An LCD screen with the "Sungkyunkwan University" logo, six green in-series connected LEDs, a remote control, and power controller switches were also affixed to the self-powered smart suit at different positions, as shown in Figure 7a–e. The schematic circuit diagram used for operating the LEDs, LCD, power controller, and remote control is shown in

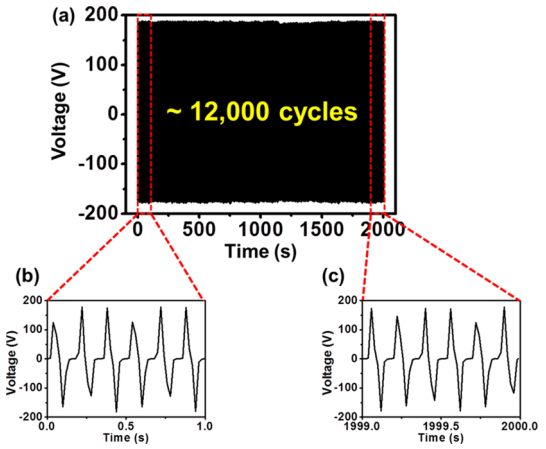

Figure 5. Mechanical durability test of the WTNG. (a) Output voltages with continuous application of cycled compressive force to the four-layer-stacked WTNG over 12 000 cycles. (b) Voltage outputs at the initial stage. (c) Voltage outputs after 12 000 cycles.

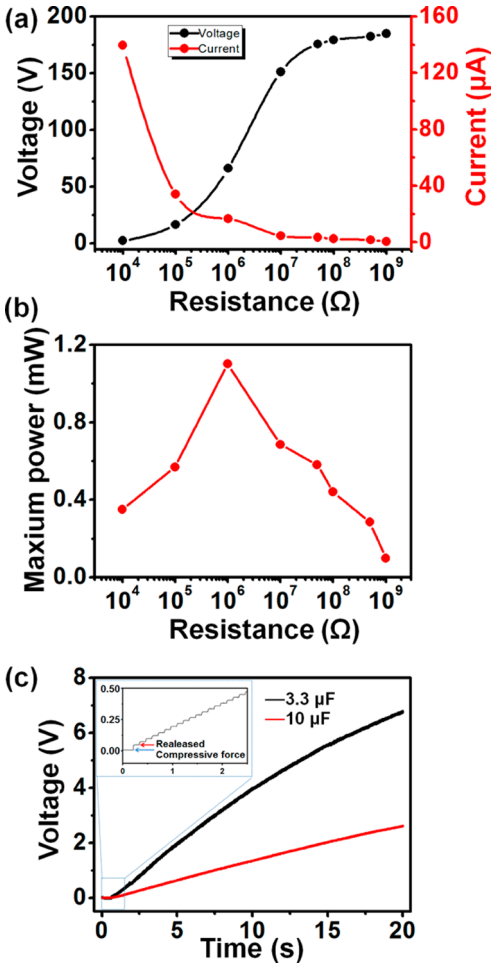

Figure 6. (a) Voltage and current outputs from the stacked WTNG as a function of different resistors as external loads. (b) Dependence of the maximum power on external load resistances. (c) Charging curves of 3.3 and 10 μF capacitors charged by the power generated from the stacked WTNG and charging steps of the 3.3 μF capacitor (inset).

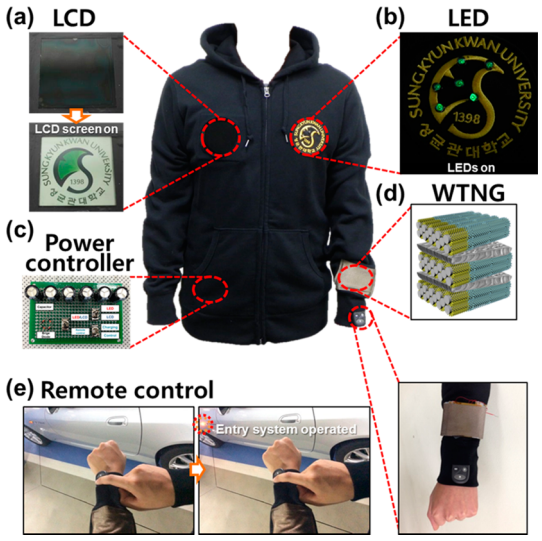

Figure 7. Self-powering of a commercial LCD, LEDs, and a remote control (keyless vehicle entry system) embedded in the "self-powered smart suit" using the WTNG. (a) The LCD lit up and displaying the "Sungkyunkwan University" logo using the output power generated from the WTNG. (b) Six LEDs simultaneously lit up by the power output generated from the WTNG directly. (c) Power controller switches affixed in a pocket. (d) Multilayer-stacked WTNG inserted on the jacket sleeve. (e) Operation of a remote control used for a keyless vehicle entry system using a commercial capacitor (1200 μF) charged only by the WTNG without any help from an external charging source.

Figure S7. The LCD screen turned on when the output power generated by the WTNG exceeded the threshold voltage of the LCD screen, as shown in Figure 7a. The rectified output power generated from the WTNG was sufficient to simultaneously activate all six LEDs (Figure 7b). Finally, a remote control used for a keyless vehicle entry system was operated using a commercial capacitor (1200 μF) charged only by the WTNG without any help from an external charging source. Figure 7e depicts the remote control keyless entry activated when the corresponding switch is turned on.

CONCLUSIONS

In conclusion, we have demonstrated the high electric-power-generating performance and mechanical robustness of fully flexible, foldable WTNGs with PDMS nanopatterns based on ZnO NRs formed on a Ag-coated textile template. A high output voltage and output current of about 120 V and 65 μA, respectively, were observed from the nanopatterned PDMS-based WTNG, while an output voltage and output current of 30 V and 20 μA were obtained by the non-nanopatterned flat PDMS-based WTNG under the same mechanical compressive force of 10 kgf. In addition, very high voltage and current outputs with an average value of 170 V and 120 μA, respectively, were obtained from the four -layer-stacked WTNG under the same normal compressive force. The output power was maximized at around 1.1 mW at an external resistance of about 1 MΩ. It was found that there are no significant differences in the output voltages measured from the multilayer-stacked WTNG over 12 000 cycles, confirming the excellent mechanical durability of the WTNG in this work. Finally, we successfully demonstrated the self-powered operation of LEDs, the LCD, and the keyless vehicle entry system only with the output power of our WTNG without any help from external power sources, which proves potential applications of WTNGs in self-powered smart clothes, health care monitoring and self-powered wearable devices, and even personal electronics.

EXPERIMENTAL SECTION

Fabrication of the Nanopatterned PDMS Structure on Textile. Commercially available Ag-coated woven textiles were used for fabricating WTNGs. The PDMS nanopatterns were fabricated on ZnO NRs. For the formation of a ZnO seed layer, zinc acetate [$Zn(CH_3COO)_2 \cdot 2H_2O$, 0.03 M] was dissolved in ethanol (100 mL) and used as a seed solution. The Ag-coated textile substrate was dipped for 10 min to form a ZnO seed layer, then dried on a hot plate at 100 °C. The dipping and annealing step was repeated three times. ZnO NRs were grown on the ZnO seed layer/Ag-coated textile substrate in a mixture of zinc nitrate hexahydrate [$Zn(NO_3)_2 \cdot 6H_2O$, 0.025 M], hexamethylenetetramine (0.025 M), and deionized water (500 mL). The growth of the ZnO NRs was done at 95 °C for 3 h. To realize the nanopatterning, a PDMS solution was coated onto the ZnO NR arrays using a dip-coating process, followed by a thermal anneal at 80 °C for 2 h.

Characterization and Measurements. The morphology and structural properties of ZnO NRs and nanopatterned PDMS were examined by FE-SEM. A pushing tester (Labworks Inc., model no. pa-151 and ET-126B-4) was used to apply programmed forces to the WTNGs. A Tektronix DPO 3052 digital phosphor oscilloscope and low-noise current amplifier (model no. SR570, Stanford Research Systems, Inc.) were used to detect the output signals generated from the WTNG.

Conflict of Interest: The authors declare no competing financial interest.

Supporting Information Available: FE-SEM images of the Ag-coated knitted textile and the textile stretched with an external force; FE-SEM images of uniformly well-aligned ZnO NRs on the textile substrate with different magnification; output voltage and current signals obtained from the WTNG in forward and reverse connections; voltage and current outputs of the multilayer-stacked WTNG as a function of the applied force; strain distributions of ZnO NR arrays and ZnO NR array-templated PDMS nanopatterns on the same Ag-coated textiles that are simulated by the COMSOL Multiphysics software; photographs of the circuit board for external load resistance-dependent measurements and the power controller for the operation of LCD and LEDs; the remote control and electrical circuit diagram of the power controller. This material is available free of charge *via* the Internet at http://pubs.acs.org.

Acknowledgment. This work was financially supported by Basic Science Research Program (2012R1A2A1A01002787, 2009-0083540) and the Center for Advanced Soft-Electronics as Global Frontier Project (2013M3A6A5073177) through the National Research Foundation (NRF) of Korea Grant funded by the Ministry of Science, ICT & Future Planning.

REFERENCES AND NOTES

1. Zeng, W.; Shu, L.; Li, Q.; Chen, S.; Wang, F.; Tao, M.-X. Fiber-Based Wearable Electronics: A Review of Materials, Fabrication, Devices, and Applications. *Adv. Mater.* **2014**, *26*, 5310–5336.
2. Li, Z.; Wang, Z. L. Air/Liquid-Pressure and Heartbeat-Driven Flexible Fiber Nanogenerators as a Micro/Nano-Power Source or Diagnostic Sensor. *Adv. Mater.* **2011**, *23*, 84–89.
3. Granero, A. J.; Wagner, P.; Wagner, K.; Razal, J. M.; Wallace, G. G.; in het Panhuis, M. Highly Stretchable Conducting SIBS-P3HT Fibers. *Adv. Funct. Mater.* **2011**, *21*, 955–962.
4. Cherenack, K.; Zysset, C.; Kinkeldei, T.; Münzenrieder, N.; Tröster, G. Woven Electronic Fibers with Sensing and Display Functions for Smart Textiles. *Adv. Mater.* **2010**, *22*, 5178–5182.
5. Wang, Z. L.; Song, J. Piezoelectric Nanogenerators Based on Zinc Oxide Nanowire Arrays. *Science* **2006**, *312*, 242–246.
6. Lee, J.-H.; Lee, K. Y.; Gupta, M. K.; Kim, T. Y.; Lee, D.-Y.; Oh, J.; Ryu, C.; Yoo, W. J.; Kang, C.-Y.; Yoon, S.-J.; Yoo, J.-B.; Kim, S.-W. Highly Stretchable Piezoelectric-Pyroelectric Hybrid Nanogenerator. *Adv. Mater.* **2014**, *26*, 765–769.
7. Chung, S. Y.; Kim, S.; Lee, J.-H.; Kim, K.; Kim, S.-W.; Kang, C.-Y.; Yoon, S.-J.; Kim, Y. S. All-Solution-Processed Flexible Thin Film Piezoelectric Nanogenerator. *Adv. Mater.* **2012**, *24*, 6022–6027.
8. Zheng, Q.; Shi, B.; Fan, F.; Wang, X.; Yan, L.; Yuan, W.; Wang, S.; Liu, H.; Liu, Z.; Wang, Z. L. *In Vivo* Powering of Pacemaker by Breathing-Driven Implanted Triboelectric Nanogenerator. *Adv. Mater.* **2014**, *26*, 5851–5856.
9. Lee, S.; Hinchet, S.; Lee, Y.; Yang, Y.; Lin, Z.-H.; Ardila, G.; Montès, L.; Mouis, M.; Wang, Z. L. Ultrathin Nanogenerators as Self-Powered/Active Skin Sensors for Tracking Eye Ball Motion. *Adv. Funct. Mater.* **2014**, *24*, 1163–1168.
10. Li, Z.; Zhu, G.; Yang, R.; Wang, A. C.; Wang, Z. L. Muscle-Driven *in Vivo* Nanogenerator. *Adv. Mater.* **2010**, *22*, 2534–2537.
11. Dagdeviren, C.; Yang, B. D.; Su, Y.; Tran, P. L.; Joe, P.; Anderson, E.; Xia, J.; Doraiswamy, V.; Dehdashti, B.; Feng, X.; *et al*. Conformal Piezoelectric Energy Harvesting and Storage from Motions of the Heart, Lung, and Diaphragm. *Proc. Natl. Acad. Sci. U.S.A.* **2014**, *111*, 1927–1932.
12. Wang, X.; Liu, J.; Song, J.; Wang, Z. L. Integrated Nanogenerators in Biofluid. *Nano Lett.* **2007**, *7*, 2475–2479.
13. Fan, F.-R.; Tian, Z.-Q.; Wang, Z. L. Flexible Triblelectric Generator!. *Nano Energy* **2012**, *1*, 328–334.
14. Fan, F.-R.; Lin, L.; Zhu, G.; Wu, W.; Zhang, R.; Wang, Z. L. Transparent Triboelectric Nanogenerators and Self-Powered Pressure Sensors Based on Micropatterned Plastic Films. *Nano Lett.* **2012**, *12*, 3109–3114.
15. Wang, S.; Lin, L.; Wang, Z. L. Nanoscale Triboelectric-Effect-Enabled Energy Conversion for Sustainably Powering Portable Electronics. *Nano Lett.* **2012**, *12*, 6339–6346.
16. Zhu, G.; Lin, Z.-H.; Jing, Q.; Bai, P.; Pan, C.; Yang, Y.; Zhou, Y.; Wang, Z. L. Toward Large-Scale Energy Harvesting by a Nanoparticle-Enhanced Triboelectric Nanogenerator. *Nano Lett.* **2013**, *13*, 847–853.
17. Wang, S.; Lin, L.; Xie, Y.; Jing, Q.; Niu, S.; Wang, Z. L. Sliding-Triboelectric Nanogenerators Based on in-Plane Charge-Separation Mechanism. *Nano Lett.* **2013**, *13*, 2226–2233.
18. Lin, L.; Wang, S.; Xie, Y.; Jing, Q.; Niu, S.; Hu, Y.; Wang, Z. L. Segmentally Structured Disk Triboelectric Nanogenerator for Harvesting Rotational Mechanical Energy. *Nano Lett.* **2013**, *13*, 2916–2923.
19. Bai, P.; Zhu, G.; Liu, Y.; Chen, J.; Jing, Q.; Yang, W.; Ma, J.; Zhang, G.; Wang, Z. L. Cylindrical Rotating Triboelectric Nanogenerator. *ACS Nano* **2013**, *7*, 6361–6366.
20. Chen, J.; Zhu, G.; Yang, W.; Jing, Q.; Bai, P.; Yang, Y.; Hou, T.-C.; Wang, Z. L. Harmonic-Resonator-Based Triboelectric Nanogenerator as a Sustainable Power Source and a Self-Powered Active Vibration Sensor. *Adv. Mater.* **2013**, *25*, 6094–6099.
21. Niu, S.; Liu, Y.; Wang, S.; Lin, L.; Zhou, Y. S.; Hu, Y.; Wang, Z. L. Theory of Sliding-Mode Triboelectric Nanogenerators. *Adv. Mater.* **2013**, *25*, 6184–6193.
22. Yang, Y.; Zhou, Y. S.; Zhang, H.; Liu, Y.; Lee, S.; Wang, Z. L. A Single-Electrode Based Triboelectric Nanogenerator as Self-Powered Tracking System. *Adv. Mater.* **2013**, *25*, 6594–6601.
23. Zhang, H.; Yang, Y.; Su, Y.; Chen, J.; Adams, K.; Lee, S.; Hu, C.; Wang, Z. L. Triboelectric Nanogenerator for Harvesting Vibration Energy in Full Space and as Self-Powered Acceleration Sensor. *Adv. Funct. Mater.* **2014**, *24*, 1401–1407.
24. Yang, Y.; Zhang, H.; Liu, R.; Wen, X.; Hou, T.-C.; Wang, Z. L. Fully Enclosed Triboelectric Nanogenerators for Applications in Water and Harsh Environments. *Adv. Energy Mater.* **2013**, *3*, 1563–1568.
25. Bai, P.; Zhu, G.; Lin, Z.-H.; Jing, Q.; Chen, J.; Zhang, G.; Ma, J.; Wang, Z. L. Integrated Multilayered Triboelectric Nanogenerator for Harvesting Biomechanical Energy from Human Motions. *ACS Nano* **2013**, *7*, 3713–3719.
26. Yang, W.; Chen, J.; Zhu, G.; Yang, J.; Bai, P.; Su, Y.; Jing, Q.; Cao, X.; Wang, Z. L. Harvesting Energy from the Natural Vibration of Human Walking. *ACS Nano* **2013**, *7*, 11317–11324.
27. Yang, Y.; Zhang, H.; Lin, Z.-H.; Zhou, Y. S.; Jing, Q.; Su, Y.; Yang, J.; Chen, J.; Hu, C.; Wang, Z. L. Human Skin Based Triboelectric Nanogenerators for Harvesting Biomechanical Energy and as Self-Powered Active Tactile Sensor System. *ACS Nano* **2013**, *7*, 9213–9222.
28. Jing, Q.; Zhu, G.; Wu, W.; Bai, P.; Xie, Y.; Han, R. P. S.; Wang, Z. L. Self-Powered Triboelectric Velocity Sensor for Dual-Mode Sensing of Rectified Linear and Rotary Motions. *Nano Energy* **2014**, *10*, 305–312.
29. Lee, S.; Lee, Y.; Kim, D.; Yang, Y.; Lin, L.; Lin, Z.-H.; Hwang, W.; Wang, Z. L. Triboelectric Nanogenerator for Harvesting Pendulum Oscillation Energy. *Nano Energy* **2013**, *2*, 1113–1120.
30. Xie, Y.; Wang, S.; Niu, S.; Lin, L.; Jing, Q.; Su, Y.; Wu, Z.; Wang, Z. L. Multi-Layered Disk Triboelectric Nanogenerator for Harvesting Hydropower. *Nano Energy* **2014**, *6*, 129–136.
31. Liang, Q.; Zhanga, Z.; Yan, X.; Gu, Y.; Zhao, Y.; Zhang, G.; Lu, S.; Liao, Q.; Zhang, Y. Functional Triboelectric Generator as Self-Powered Vibration Sensor with Contact Mode and Non-Contact Mode. *Nano Energy* **2014**, http://dx.doi.org/10.1016/j.nanoen.2014.07.010.
32. Wen, X.; Su, Y.; Yang, Y.; Zhang, H.; Wang, Z. L. Applicability of Triboelectric Generator over a Wide Range of Temperature. *Nano Energy* **2014**, *4*, 150–156.
33. Yang, Y.; Lin, L.; Zhang, Y.; Jing, Q.; Hou, T.-C.; Wang, Z. L. Self-Powered Magnetic Sensor Based on a Triboelectric Nanogenerator. *ACS Nano* **2012**, *6*, 10378–10383.
34. Lin, Z.-H.; Zhu, G.; Zhou, Y. S.; Yang, Y.; Bai, P.; Chen, J.; Wang, Z. L. A Self-Powered Triboelectric Nanogenerator for Mercury Ion Detection. *Angew. Chem., Int. Ed.* **2013**, *52*, 5065–5069.
35. Zhang, H.; Yang, Y.; Hou, T.-C.; Su, Y.; Hu, C.; Wang, Z. L. Triboelectric Nanogenerator Built inside Clothes for Self-Powered Glucose Biosensors. *Nano Energy* **2013**, *2*, 1019–1024.
36. Zhu, G.; Pan, C.; Guo, W.; Chen, C.-Y.; Zhou, Y.; Yu, R.; Wang, Z. L. Triboelectric-Generator-Driven Pulse Electrodeposition for Micropatterning. *Nano Lett.* **2012**, *12*, 4960–4965.
37. Lee, M.; Chen, C.-Y.; Wang, S.; Cha, S. N.; Park, Y. J.; Kim, J. M.; Chou, L.-J.; Wang, Z. L. A Hybrid Piezoelectric Structure for Wearable Nanogenerators. *Adv. Mater.* **2012**, *24*, 1759–1764.
38. Kim, H.; Kim, S. M.; Son, H.; Kim, H.; Park, B. I.; Ku, J. Y.; Sohn, J. I.; Im, K.; Jang, J. E.; Park, J.-J.; *et al*. Enhancement of Piezoelectricity *via* Electrostatic Effects on a Textile Platform. *Energy Environ. Sci.* **2012**, *5*, 8932–8936.
39. Lee, S. H.; Lee, J. S.; Ko, W. B.; Cha, S. N.; Sohn, J.; Kim, J. M.; Park, J. G.; Park, Y.; Hong, J. P. Solution-Processed Ag-Doped ZnO Nanowires Grown on Flexible Polyester for Nanogenerator Applications. *Nanoscale* **2013**, *5*, 9609–9614.
40. Zhong, J.; Zhang, Y.; Zhong, Q.; Hu, Q.; Hu, B.; Wang, Z. L.; Zhou, J. Fiber-Based Generator for Wearable Electronics and Mobile Medication. *ACS Nano* **2014**, *8*, 6273–6280.

41. Zhou, T.; Zhang, C.; Han, C. B.; Fan, F. R.; Tang, W.; Wang, Z. L. Woven Structured Triboelectric Nanogenerator for Wearable Devices. *ACS Appl. Mater. Interfaces* **2014**, *6*, 14695–14701.
42. Jung, S.; Lee, J.; Hyeon, T.; Lee, M.; Kim, D.-H. Fabric-Based Integrated Energy Devices for Wearable Activity Monitors. *Adv. Mater.* **2014**, *26*, 6329–6334.
43. Lee, K. Y.; Chun, J.; Lee, J.-H.; Kim, K. N.; Kang, N.-R.; Kim, J.-Y.; Kim, M. H.; Shin, K.-S.; Gupta, M. K.; Baik, J. M.; *et al*. Hydrophobic Sponge Structure-Based Triboelctric Nanogenerator. *Adv. Mater.* **2014**, *26*, 5037.